*Journal of Ceramic Processing Research. Vol. 8, No. 2, pp. 98~102 (2007)*

J O U R N A L O F
**Ceramic Processing Research**

# Post-CMP dry etching for the removal of the nanoscale subsurface damage layer from a single crystal $La_3Ga_5SiO_{14}$ for a high quality wide band SAW filter device

**D.M. Lee, S. Hwang[a], B.W. Lee[b], K.B. Shim[c], S.J. Pearton[d] and H. Cho***

*Department of Nanosystem and Nanoprocess Engineering, Pusan National University, Kyungnam 627-706, Korea*
*[a]Department of Nanomedical Engineering, Pusan National University, Kyungnam 627-706, Korea*
*[b]Department of Materials Engineering, Korea Maritime University, Busan 606-791, Korea*
*[c]Department of Ceramic Engineering, Hanyang University, Seoul 133-791, Korea*
*[d]Department of Materials Science and Engineering, University of Florida, Gainesville, FL 32611, USA*

**The nanoscale subsurface damage layer induced on a single crystal $La_3Ga_5SiO_{14}$ during the Chemical Mechanical Polishing (CMP) process for surface finishing is removed by a post-CMP dry etching in $Cl_2$/Ar inductively coupled plasmas. The electrical conductivity is recovered to the initial value (~$1\times10^{-4}$ $\Omega^{-1}\cdot cm^{-1}$) measured before being CMP-processed with a colloidal silica slurry at etch depths of 43-68 nm, while maintaining a smooth surface morphology. The depth of the subsurface damage layer formed in a langasite single crystal initially increases as a downward force applied to a single crystal $La_3Ga_5SiO_{14}$ during the CMP process increases, and then saturates at depths ~68 nm, indicating that the subsurface damage layer induced by the mechanical stress does not form to a depth beyond a critical level.**

**Key words: subsurface damage layer, single crystal $La_3Ga_5SiO_{14}$, chemical mechanical polishing, post-CMP dry etching, $Cl_2$/Ar inductively coupled plasmas, electrical conductivity recovery.**

## Introduction

A langasite ($La_3Ga_5SiO_{14}$, LGS) single crystal is considered as the most promising piezoelectric substrate for wide band surface acoustic wave (SAW) filter devices in wireless-communication technology, such as for wide-band-code division multiple access (W-CDMA). Langasite has an electromechanical coupling factor approximately three times larger than that of quartz and an especially high temperature stability up to 1000 °C and a larger frequency stability range [1-9]. In the fabrication of langasite SAW filter devices, the surface finish process while maintaining flatness and parallelism of the crystal blanks is extremely important since the insertion loss is determined by the properties of the surface upon which the surface acoustic wave travels. To date chemical mechanical polishing (CMP) has played an important role in fine-tuning of the thickness and surface morphology of langasite single crystal wafers [10-12].

However, it has been recently found that the CMP process induces a nanoscale subsurface damage layer to the wafer that causes degradation in the electrical property of the final devices [13-15]. It is important to develop a process, which can remove the subsurface damage layer with high efficiency and reproducibility to realize high quality langasite-based wide band SAW filter devices.

In this study we report on the removal of the CMP-induced subsurface damage layer formed on a langasite wafer and the effect of the downwards force on the structural stability of the subsurface damage layer using a high density plasma technique ($Cl_2$/Ar inductively coupled plasmas) by establishing the process window where we can produce practical and controllable etch rates while maintaining a smooth surface morphology.

## Experimental

Single crystalline langasite wafers 3 inches in diameter grown by the Czochralski method were CMP-processed with 0.045 μm colloidal silica slurry and the downwards force applied to the wafer was varied from 5 to 25 N. Samples were masked with either Apiezon wax or $SiO_2$. Post-CMP dry etching was performed in a Plasma-Therm ICP 790 reactor utilizing a 3-turn coil inductively coupled plasma (ICP) source operating at 2 MHz and power up to 1500 W, and the samples were thermally bonded to a Si carrier wafer that was mechanically clamped to a He backside cooled, rf powered (13.56 MHz, up to 450 W) chuck. $Cl_2$/Ar or $CF_4$/Ar inductively coupled plasma was employed to etch langasite wafers and the total gas load was fixed at 15 standard cubic centimeters per minute. After removal of the mask material etch rate, surface morphology and

*Corresponding author:
Tel : +82-55-350-5286
Fax: +82-55-350-5653
E-mail: hyuncho@pusan.ac.kr

near-surface stoichiometry were characterized by stylus profilometry measurements, scanning electron microscopy (SEM), atomic force microscopy (AFM) and Auger electron spectroscopy (AES). The depth profile of subsurface damage layer was examined by monitoring the changes in the electrical properties of a langasite wafer with variation of etched depth from the surface.

## Results and Discussion

Figure 1 shows the langasite etch rates as a function of plasma composition in either $Cl_2$/Ar or $CF_4$/Ar ICP discharges, with 750 W source power, 250 W rf power and 2 mTorr (0.267 Pa) pressure. In $Cl_2$/Ar plasma chemistries, the etch rate is a strong function of plasma composition, indicating the presence of a strong chemical component of the etching. The etch rate increases monotonically with $Cl_2$ content in the discharge due to the higher density of the reactive atomic chlorine neutrals in the plasma and maximum etch rate ~160 nm/minute is obtained in a pure $Cl_2$ discharge. The dc self-bias, which controls the average energy of the incident ions, continues to increase with $Cl_2$ percentage since the $Cl_2$ is electronegative and there will be relatively fewer positive ions present. By contrast, $CF_4$/Ar ICP discharges produce much lower etch rates (max. ~60 nm/minute) than with $Cl_2$/Ar mixtures under the conditions examined most likely due to the lower volatility of the metal fluoride reaction products except $SiF_4$ (compare boiling points of potential etch products; $LaCl_3$: 1812 $^oC$, $LaF_3$: 2327 $^oC$, $GaCl_2$: 535 $^oC$, $GaCl_3$: 201 $^oC$, $GaF_3$: ~950 $^oC$, $SiCl_4$: 57.65 $^oC$, $SiF_4$: -80 $^oC$).

Figure 2 shows the ICP source power dependence of the langasite etch rate at a fixed plasma composition ($10Cl_2$/5Ar or $10CF_4$/5Ar) and rf chuck power (250 W). Under high density plasma conditions, the dissociation efficiency of the discharges is controlled by the source power at fixed rf chuck power conditions [16, 17]. Increasing the source power produces a higher ion flux

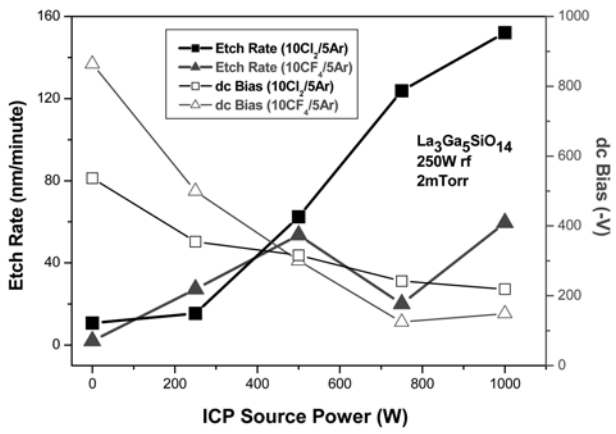


**Fig. 2.** $La_3Ga_5SiO_{14}$ etch rate as a function of ICP source power in either $10Cl_2$/5Ar or $10CF_4$/5Ar ICP discharges (250 W rf power, 2 mTorr (0.267 Pa)).

but decreases the average incident ion energy, indicated by the sum of the plasma potential (~25-30 eV under our conditions) and the dc self-bias. The langasite etch rate increases as the source power increases even though the dc self-bias is suppressed significantly due to the enhanced metal chloride or metal fluoride etch products (presumably $LaCl_x$, $GaCl_x$, $SiCl_x$, $LaF_x$, $GaF_x$, $SiF_x$ and $O_2$) formation and subsequent ion-assisted desorption. However, there is a trade-off between the increased ion flux and decreased ion energy in the higher source power region (> 500 W) in $10CF_4$/5Ar ICP discharges indicating the etching is limited by ion-assisted desorption of metal fluoride etch products under these conditions.

The effect of rf chuck power on the langasite etch rate at a fixed plasma composition ($10Cl_2$/5Ar or $10CF_4$/5Ar) and source power (750 W) is shown in Fig. 3. In $10Cl_2$/5Ar discharges the langasite etch rate initially increases up to moderate rf chuck power conditions (250 W) and then decreases or saturates at higher power conditions. This type of behavior is some-

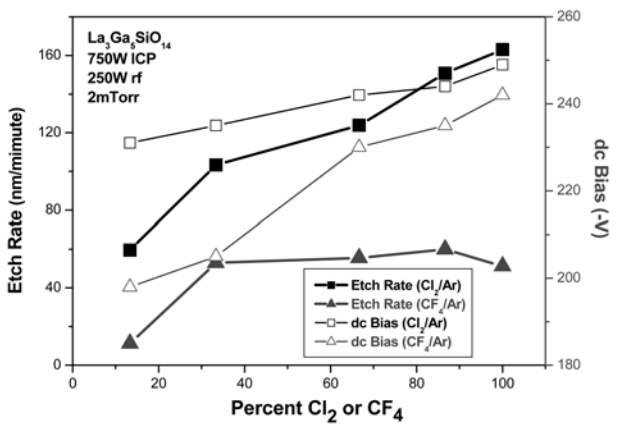


**Fig. 1.** $La_3Ga_5SiO_{14}$ etch rate as a function of plasma composition in either $Cl_2$/Ar or $CF_4$/Ar ICP discharges (750 W source power, 250 W rf power, 2 mTorr (0.267 Pa)).

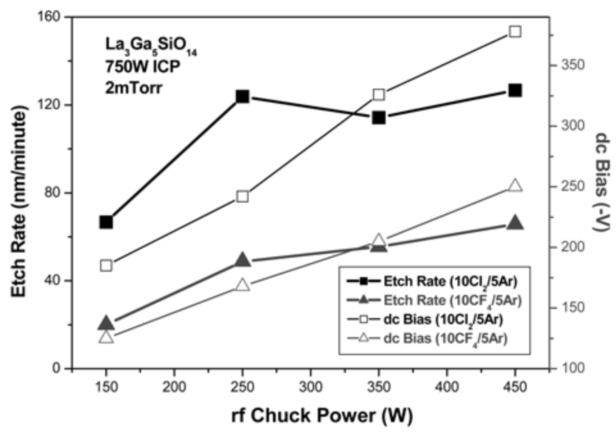


**Fig. 3.** $La_3Ga_5SiO_{14}$ etch rate as a function of rf chuck power in either $10Cl_2$/5Ar or $10CF_4$/5Ar ICP discharges (750 W source power, 2 mTorr (0.267 Pa)).

what common in the dry etching of III-V materials, and is usually ascribed to ion-enhanced removal of the active fluorine species from the langasite surface before they can react, if the ion energy exceeds a particular value [18, 19]. By contrast, the langasite etch rate increases monotonically as the rf chuck power increases in $10CF_4/5Ar$ ICP discharges due to the enhanced ion-assisted desorption of metal fluoride etch products, indicating the presence of a strong physical component of the etching.

In addition to obtaining a practical and controllable etch rate from langasite wafers, the other important issue is surface morphology of the etched wafers since the ICP etching we discuss here is a post-CMP process for the removal of the CMP-induced subsurface damage layer. The normalized roughness data of ICP-etched langasite surfaces as a function of source power are shown in Figs. 4 at a fixed plasma composition ($10Cl_2$/5Ar or $10CF_4/5Ar$) and rf power (250 W). In each case, the etch depth was ~300 nm. In $10Cl_2/5Ar$ discharges the etched langasite surfaces show better or similar root-mean-square (RMS) roughness values than the unetched control sample (RMS roughness: 0.809 nm) under most of conditions examined. By sharp contrast, a severe degradation in surface morphology was observed after etching in $CF_4/Ar$ ICP discharges since the etching is dominated by the physical component of the etching, as discussed earlier, under most of the conditions examined.

Similar data is shown in Fig. 5 for langasite samples etched in either $10Cl_2/5Ar$ or $10CF_4/5Ar$ ICP discharges at different rf chuck powers. In the case of $10Cl_2/5Ar$ mixtures, there is consistent smoothing of the surface occurring, as also seen in the data in Fig. 4, up to relatively high rf power conditions. At higher rf power condition (450W), the langasite surface gets rougher than the unetched control sample, most likely due to severe ion bombardment with higher ion energies on the surface. Comparing the etch characteristics of langasite wafers in both of $Cl_2/Ar$ and $CF_4/Ar$ ICP discharges, $Cl_2/Ar$ ICP etching seems to be a very attractive post-CMP process since it can produce more practical etch rates while maintaining smooth surface morphology.

The pattern transfer was extremely anisotropic under a wide range of conditions, Figure 6 shows SEM micrographs of features etched into langasite (the mask layer is still in place) using $10Cl_2/5Ar$ discharges with a 500 W source power and 250W rf chuck power. The etched langasite wafer shows a smooth surface morphology, indicating equi-rate removal of the etch products, and a vertical sidewall profile is obtained.

AES surface scans of the unetched langasite control sample and one etched in $10Cl_2/5Ar$ discharges with a 500 W source power and 250 W rf chuck power are

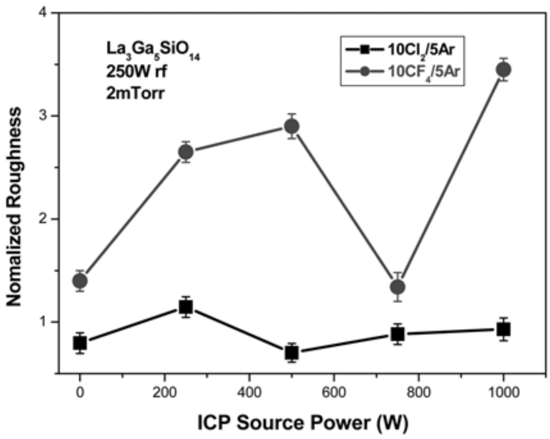


**Fig. 4.** Dependence of $La_3Ga_5SiO_{14}$ normalized etched surface roughness on ICP source power in either $10Cl_2/5Ar$ or $10CF_4/5Ar$ ICP discharges (250 W rf power, 2 mTorr (0.267 Pa)).

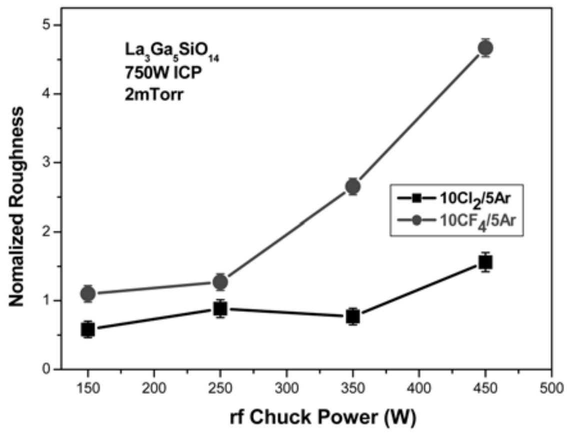


**Fig. 5.** Dependence of $La_3Ga_5SiO_{14}$ normalized etched surface roughness on rf chuck power in either $10Cl_2/5Ar$ or $10CF_4/5Ar$ ICP discharges (750 W source power, 2 mTorr (0.267 Pa)).

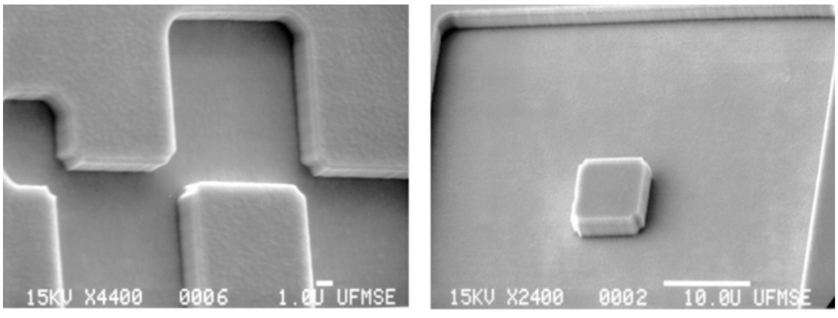


**Fig. 6.** SEM micrographs features etched into $La_3Ga_5SiO_{14}$ using $10Cl_2/5Ar$, 500 W source power, 250 W rf chuck power discharges.

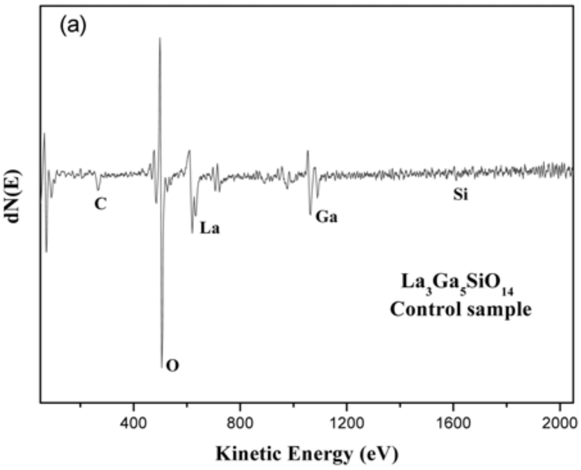


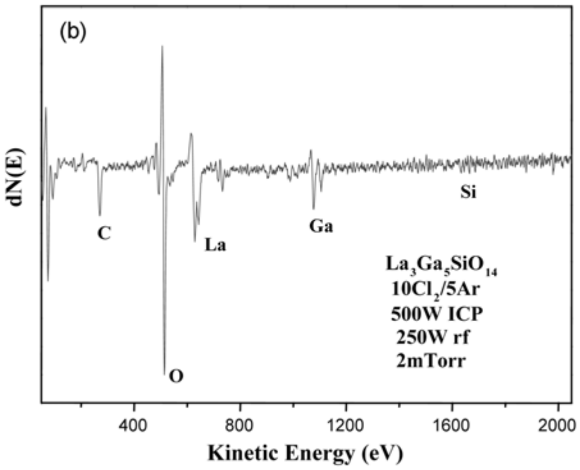


**Fig. 7.** AES surface scans of (a) the unetched and (b) etched $La_3Ga_5SiO_{14}$ in $10Cl_2/5Ar$ discharges (500 W source power, 250 W rf power).

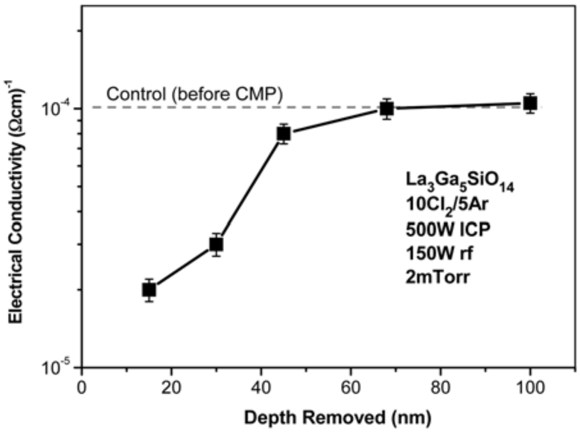


**Fig. 8.** Dependence of electrical conductivity of $La_3Ga_5SiO_{14}$ wafers as a function of etch depth removed ($10Cl_2/5Ar$, 500 W source power, 150 W rf power, 2 mTorr (0.267 Pa)).

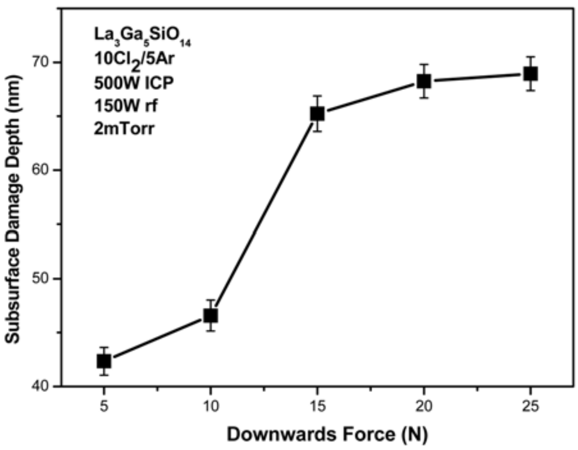


**Fig. 9.** Dependence of subsurface damage depth as a function of down force applied to $La_3Ga_5SiO_{14}$ during CMP process ($10Cl_2/5Ar$, 500 W source power, 150 W rf power, 2 mTorr (0.267 Pa)).

shown in Fig. 7. There is no significant change in stoichiometry detected before and after etching and the near surface stoichiometry of langasite is found not to be affected by $Cl_2/Ar$ ICP etching.

Figure 8 shows the electrical conductivity of langasite wafers examined by Hall measurements as a function of etch depth removed from the surface at a fixed plasma composition ($10Cl_2/5Ar$) and relatively lower power condition (500 W source power, 150 W rf power). The recovery in electrical conductivity is observed as the etch depth increases indicating that the subsurface damage layer is removed by $Cl_2/Ar$ inductively coupled plasma etching, and is restored to the initial value ($\sim 1\times10^{-4}\ \Omega^{-1}\cdot cm^{-1}$) measured before being CMP-processed with 0.045 μm colloidal silica slurry and a 15 N downwards force where we can obtain the lowest surface roughness value at an etch depth ~68 nm. It is clear that the subsurface damage layer is induced in the langasite wafer surface by the CMP process with a depth of ~68 nm and may be successfully removed by $Cl_2/Ar$ ICP etching at relatively lower power conditions while maintaining smooth surface morphology.

The effect of the downwards force applied to langasite wafers during the CMP process on the structural stability of the subsurface damage layer is shown in Fig. 9. In each case, the structural stability of subsurface damage layer is determined by monitoring the etch depth where the electrical conductivity is recovered to $\sim 1\times10^{-4}\ \Omega^{-1}\cdot cm^{-1}$. The depth of the subsurface damage layer is a strong function of the downwards force applied during the CMP process. The depth of the subsurface damage layer formed in langasite initially increases as the downwards force increases and then saturates at a depth ~68 nm indicating that the subsurface damage layer induced by the mechanical stress does not form at depths beyond a critical level.

## Summary and Conclusions

$Cl_2/Ar$ inductively coupled plasma (ICP) discharges produce practical and controllable etch rates for single crystalline $La_3Ga_5SiO_{14}$ wafers. A maximum etch rate ~160 nm/minute was achieved either at a relatively high source power (~1000 W) or with high $Cl_2$ content conditions in $Cl_2$/Ar discharges and the etched langasite surfaces show similar or better RMS roughness values than the unetched control sample under most of the conditions examined. By contrast, a $CF_4$/Ar inductively coupled plasma produces much lower etch rates than $Cl_2$/Ar discharges and a severe degradation in surface morphology was observed after etching. The pattern transfer in $Cl_2$/Ar ICP discharges is extremely anisotropic under a wide range of conditions and the near surface stoichiometry of an etched langasite wafer is found not to be affected by ICP etching. The nanoscale CMP-induced subsurface damage layer was successfully removed by a post-CMP dry etching in $Cl_2$/Ar ICP plasmas and the electrical conductivity was restored to the initial values ($\sim 1\times10^{-4}\ \Omega^{-1}\cdot cm^{-1}$) measured before the CMP-process at an etch depth of ~68 nm. The downwards force applied to a langasite wafer during the CMP process has a strong effect on the structural stability of the subsurface damage layer and a subsurface damage layer induced by the mechanical stress does not form at depths beyond a critical level (~68 nm). It is found that high density plasma (ICP) etching is a very attractive post-CMP process for removal of the CMP-induced subsurface damage layer in the fabrication of high performance langasite-based SAW filter devices.

## Acknowledgments

This work was supported by the Korea Research Foundation Grant funded by the Korean Government (MOEHRD) (R05-2004-000-10952-0).

## References

1. M. Honal, R. Fachberger, T. Holzheu, E. Riha, E. Born, P. Pongratz, and A. Bausewein, IEEE/EIA Int'l. Freq. Control Symp. (2000) 113-118.
2. B.A. Dorogovin, S. Yu. Stepanov, A.B. Doubovski, and A.A. Tsegleev, IEEE/EIA Int'l. Freq. Control Symp. (2000) 169-173.
3. C. Robert and G.E. Hague, IEEE/EIA Int'l. Freq. Control Symp. (2000) 191-194.
4. D.C. Malocha, M.P. da Gunha, R.C. Smythe, S. Fredrick, M. Chou, R. Helmbold, and Y.S. Zhou, IEEE/EIA Int'l. Freq. Control Symp. (2000) 200-205.
5. S.-Q. Wang, J. Harada, and S. Uda, J. Crystal Growth 219 (2000) 263-268.
6. H. Sato, M. Kumatoriya, and T. Fujii, J. Crystal Growth 242 (2002) 177-182.
7. C. Klemenz, J. Crystal Growth 237-239 (2002) 714-719.
8. S.M. Park and D.A. Keszler, Solid State Sci. 4 (2002) 799-802.
9. S.-Q. Wang, J. Harada, and S. Uda, J. Crystal Growth 250 (2003) 463-470.
10. D.S. Lim, I. H. Yoon, and S. Danyluk, Wear 249 (2001) 397-400.
11. M. C. Jang, K. Joo, and K.H. Auh, J. Ceramic Processing Res. 1 (2000) 1-8.
12. S. Laffey, M. Hendrickson, and J.R. Vig, IEEE/EIA Int'l. Freq. Control Symp. (1994) 245-249.
13. Y. Ogita, K. Kobayashi, and H. Daio, J. Crystal Growth 210 (2000) 36-39.
14. S.H. Li and R.O. Miller, "Semiconductors and Semimetals", Vol. 63 (Academic Press, New York, 2000) p. 73.
15. C.S. Lee and C.H. Han, Sensors and Actuators A 3308 (2002) 1-6.
16. O.A. Popov, "High Density Plasma Sources" (Noyes Publications, Park Ridge, NJ 1995) p. 113.
17. C.R. Eddy and B. Molnar, J. Electron. Mater. 28 (1999) 314-319.
18. D.C. Hays, P. Leerungnawarat, S.J. Pearton, G. Archibald, and R.C. Smythe, Appl. Surface Sci. 165 (2000) 127-134.
19. C.B. Vartuli, J.D. MacKenzie, J.W. Lee, C.R. Abernathy, S.J. Pearton, and R.J. Shul, J. Appl. Phys. 80 (1996) 3705-3709.